J|A|C|S
ARTICLES
Published on Web 02/24/2007

Metallaborane Reactivity. A Stoichiometric Mechanism for the Insertion of Two Alkynes into an Iridaborane Framework via a Disposable Molybdenum Chaperone

Frédéric de Montigny,[†] Ramón Macias,[†] Bruce C. Noll,[†] Thomas P. Fehlner,*[,†] Karine Costuas,[‡] Jean-Yves Saillard,[‡] and Jean-François Halet[‡]

Contribution from the Department of Chemistry and Biochemistry, University of Notre Dame, Notre Dame, Indiana 46556, and Sciences Chimiques de Rennes, UMR 6226 CNRS-Université de Rennes 1, Avenue du Général Leclerc, F-35042 Rennes cedex, France

Received December 15, 2006; E-mail: fehlner.1@nd.edu

Abstract: Building on earlier work that showed the formation of [1-Cp*-2,2,2-$(CO)_3$-2-THF-*nido*-1,2-$IrMoB_4H_8$], **2**, from the reaction of [1-Cp*-*arachno*-1-IrB_4H_{10}], **1**, with (arene)$Mo(CO)_3$, the stoichiometric mechanism for the generation of [1-Cp*-5,6,7,8-$(R)_4$-*nido*-1,5,6,7,8-$IrC_4B_3H_3$], **8**, from the reaction of **2** with RC≡CR, R = Me, Ph, has been identified. For R = Me, the major product in solution is [1-Cp*-5,6,7,8-$(CH_3)_4$-*closo*-1,5,6,7,8-$IrC_4B_3H_3Mo(CO)_3$], **7**, which is in equilibrium with **8**. The equilibrium **8** + $Mo(THF)_3(CO)_3 \rightleftarrows$ **7** + 3THF is characterized by $\Delta H = 8$ kcal/mol and $\Delta S = 34$ cal/mol K. Density functional theory calculations carried out on **7** indicate that the $Mo(CO)_3$ moiety is weakly bound to the cluster mainly through Mo−C rather than Mo−B interactions. Under alkyne deficient conditions, the product [1-Cp*-2,2,2-$(CO)_3$-(μ-CO)-3,4-$(CH_3)_2$-*closo*-1,2,3,4-$IrMoC_2B_3H_3$], **6**, can be isolated. Solid-state structures of **1** and **2** have been reported previously, and those of **6**, **7**, and **8**, R = Me, Ph, are reported here. The evolution of products with time was monitored by ^{1}H and ^{11}B NMR and showed the formation and decay of two additional species which have been identified as the structural isomers [1-Cp*-7,7,7-$(CO)_3$-7-THF-2,3-$(CH_3)_2$-*nido*-1,7,2,3-$IrMoC_2B_3H_5$], **4**, and [5-Cp*-7,7,7-$(CO)_3$-7-THF-2,3-$(CH_3)_2$-*nido*-5,7,2,3-$IrMoC_2B_3H_5$], **5**, with the metals nonadjacent in **4** and adjacent in **5**. Circumstantial evidence suggests that **4** is the precursor to **5** and **5** is the precursor to both **6** and **7**. Cluster **2** also is a catalyst or catalyst precursor for the isomerization of olefins, namely, hex-1-ene to *cis*-hex-2-ene and tetramethyl allene to 2,4-dimethylpenta-1,3-diene. These novel results also establish that [1-Cp*-2,2,2-$(CO)_3$-2-(alkyne)-*nido*-1,2-$IrMoB_4H_8$], **3**, forms from **2** and constitutes a logical precursor to **4**. The entire process, **1** + 2alkyne = **8** + BH_3 + $2H_2$, which is promoted by (arene)$Mo(CO)_3$, constitutes an explicit example of a transition-metal-facilitated process analogous to metal-facilitated organic transformations observed in organometallic chemistry.

Introduction

The classic development of a subarea of chemistry begins with the discovery of a new compound type and proceeds through synthetic improvements and structural development to systematic examination of reactivity. The vagaries of funding and the "herd instincts" of chemists determine where the process peters out for any given area. But it is unfortunate when reactivity is totally neglected as it is in the delineation of mechanistic pathways that true understanding and some measure of control of electronic and geometric properties are achieved. All the bombast of application, application, application obscures the fact that this understanding is fundamental to the development of rational solutions to the tough practical problems modern life presents.

For the past couple of decades we, and others, have worked on transition metal−borane cluster compounds,[1−8] but it is only in the past decade that development of the synthetic chemistry has permitted a focus on reactivity with an eye to comparisons with organometallic chemistry. Perhaps the epitome of the latter is the utilization of metals to control the derivatization of an organic moiety in stoichiometric reactions or catalytic cycles.[9] Adding metals to carbon chemistry permits the modest barriers and small thermodynamic changes required for such chemistry to be achieved—deep energy wells brings chemistry to a halt and high intrinsic barriers increase the probability of competitive side reactions. Adding metals to boron chemistry should do the same; and the stepwise binding, modification, and release of a borane substrate is an attractive goal with potential practical

[†] University of Notre Dame.
[‡] University of Rennes.

(1) Barton, L.; Srivastava, D. K. In *Comprehensive Organometallic Chem. II*; Abel, E., Stone, F. G. A., Wilkinson, G., Eds.; Pergamon: New York, 1995; Vol. 1.
(2) Braunschweig, H. *Angew. Chem., Int. Ed.* **1998**, *37*, 1787.
(3) Fehlner, T. P. *Organometallics* **2000**, *19*, 2643.
(4) Kawano, Y.; Yasue, T.; Shimoi, M. *J. Am. Chem. Soc.* **1999**, *121*, 11744.
(5) Kennedy, J. D. *Prog. Inorg. Chem.* **1984**, *32*, 519.
(6) Kennedy, J. D. *Prog. Inorg. Chem.* **1986**, *34*, 211.
(7) Grimes, R. N. In *Metal Interactions with Boron Clusters*; Grimes, R. N., Ed.; Plenum: New York, 1982; p 269.
(8) Coffy, T. J.; Medford, G.; Plotkin, J.; Long, G. J.; Huffman, J. C.; Shore, S. G. *Organometallics* **1989**, *8*, 2404.
(9) Elschenbroich, C.; Salzer, A. *Organometallics*; VCH: New York, 1989.

10.1021/ja068999z CCC: $37.00

payoff. We describe one such system in which the modification of a metallaborane is mediated by coordination to a molybdenum carbonyl fragment.

Important earlier studies suggest that the present findings are part of a growing body of reaction chemistry supporting the thesis outlined above. Thus, we have the elegant series of papers in which a rhodacarborane serves as a homogeneous hydrogenation catalyst for organic substrates.[10] Closely related is the utilization of transition metal catalysts to effect derivatization of boranes and carboranes—a process that involves metal−borane interactions.[11] Properties of compounds containing metal−boron bonds are critical in the creation of B−C bonds to effect the functionalization of hydrocarbons in stoichiometric and catalytic processes.[12−14] Equally fascinating is the hydroboration of an unsaturated triosmium cluster to a metal cluster substituted boroxime ring versus an osmaborane.[15,16]

In exploring the reactivity of a class of metallaboranes[3] containing Cp*M (Cp* = η^5-C_5Me_5, M = Cr, Mo, W, Re, Ru, Co, Rh, Ir) fragments with alkynes, we were surprised to observe facile reactivity involving the borane fragment only in the case of *nido*-$(Cp^*RuH)_2B_3H_7$. For this compound, examination of the dependence of intermediates and final products on alkyne substituents as well as related experiments revealed the stoichiometric mechanism and the source of the variety of metallacarborane products.[17−22] The key structural feature of *nido*-$(Cp^*RuH)_2B_3H_7$ relative to isostructural and isoelectronic *nido*-$(Cp^*Rh)_2B_3H_7$, for which cyclotrimerization alone was observed,[23] is the "extra" two hydrogen atoms present in the ruthenaborane. These foster facile hydrometallation and/or ready incorporation of the alkyne carbon atoms into the cluster framework. Although the mechanistic evidence suggests both rhoda- and ruthenaboranes reversibly add alkyne in a first step, only the ruthenaborane with its "extra" hydrides provides a pathway to alkyne incorporation into the cluster framework.

However, "extra" hydrides are not a sufficient condition for alkyne incorporation. For example, the iridaborane, [1-Cp*-*arachno*-1-IrB_4H_{10}], **1**,[24] with six H atoms on the framework does not react with alkynes under mild conditions. Although other reasons are possible, given the high reactivity of alkynes, a low iridaborane/alkyne association constant is a likely cause. Subsequent study of this iridaborane suggested a test. That is, we found that a group 6 metal fragment could be efficiently incorporated into **1** and that the resulting *nido*-dimetallahexaborane, [1-Cp*-2,2,2-$(CO)_3$-2-THF-*nido*-1,2-$IrMoB_4H_8$], **2**, possessed a weakly coordinated THF molecule.[25] Normally such a metallaborane would lose the THF ligand and form a closo cluster; however, an octahedral $MM'B_4$ skeleton is not well suited to accommodate the four bridging hydrogen atoms required to meet the seven skeletal electron pair (sep) cluster count. As a consequence **2** can be isolated and readily undergoes displacement of THF with a variety of Lewis bases.[25] Thus, **2** is a potential reaction partner for the incorporation of alkynes, i.e., it possesses both an accessible alkyne binding site as well as "extra" skeletal H atoms. It does react, and the essentials of the overall reaction were communicated earlier.[26] We now present the full story including that of intermediates as well as experiments that reveal some of the early mechanistic details.

Results and Discussion

Scheme 1 can be used as a guide to the following sections. The synthesis as well as selected reactivity of **1** has been described earlier.[27,28] The first reaction step, **1** → **2**, as well as the structure of **2** and displacement of THF by a variety of Lewis bases is also the principal topic of an earlier paper.[25] We begin here with the isolated products, **6**, **7**, and **8** and then continue with the less precisely characterized intermediates **4** and **5**. Finally, reactions of **2** with olefins, which are unlikely to insert, are used to refine understanding of the initial alkyne adduct **3**.

Isolated Products. The reaction of **2** with excess RC≡CR, R = Me, Ph, followed by product extraction and chromatography yielded a single pure product. Solid-state X-ray structure determinations revealed that the new compounds are the eight-vertex *nido*-iridacarboranes, [1-Cp*-5,6,7,8-$(R)_4$-*nido*-1,5,6,7,8-$IrC_4B_3H_3$], **8**, with structures shown in Figure 1 (R = Me) and Figure 1 in the Supporting Information (R = Ph). The latter suffers from the presence of unresolved solvent(s); however, it is sufficient to establish the essential similarity of the Me and Ph derivative structures. The structures in the solid state are consistent with the spectroscopic data and similar to those of known examples of the compound type, e.g., the cobaltacarborane, $[Cp^*CoC_4Ph_4B_3H_3]$, as well as main group analogs.[29−31]

Simple application of the Wade/Mingos approach predicts a cluster structure based on a tricapped trigonal prism with either a five-connect or four-connect vertex unoccupied.[32−35] However, **8** is another example of an eight-vertex, 10 skeletal electron pairs (sep) cluster that adopts a more open structure. Williams has provided one rationalization (maximized charge smoothing),[36] but it now appears clear that the number of bridging H atoms is also an important factor in determining the form of the 10 sep/8 fragment cluster shape.[37,38]

(10) Belmont, J. A.; Soto, J.; King, R. E., III; Donaldson, A. J.; Hewes, J. D.; Hawthorne, M. F. *J. Am. Chem. Soc.* **1989**, *111*, 7475.
(11) Kadlecek, D. E.; Carroll, P. J.; Sneddon, L. G. *J. Am. Chem. Soc.* **2000**, *122*, 10686.
(12) Chen, H.; Hartwig, J. F. *Angew. Chem., Int. Ed.* **1999**, *38*, 3391.
(13) Chen, H.; Schlecht, S.; Semple, T. C.; Hartwig, J. F. *Science* **2000**, *287*, 1995.
(14) Duan, Z.; Hampden-Smith, M. J.; Sylwester, A. P. *Chem. Mater.* **1992**, *4*, 1146.
(15) Shore, S. G.; Jan, D.-Y.; Hsu, W.-L.; Hsu, L.-Y.; Kennedy, S.; Huffman, J. C.; Wang, T.-C. L.; Marshall, A. G. *J. Chem. Soc., Chem. Commun.* **1984**, 392.
(16) Chung, J.-H.; Knoeppel, D.; McCarthy, D.; Columbie, A.; Shore, S. G. *Inorg. Chem.* **1993**, *32*, 3391.
(17) Yan, H.; Beatty, A. M.; Fehlner, T. P. *J. Am. Chem. Soc.* **2002**, *124*, 10280.
(18) Yan, H.; Beatty, A. M.; Fehlner, T. P. *Angew. Chem., Int. Ed.* **2001**, *40*, 4498.
(19) Yan, H.; Beatty, A. M.; Fehlner, T. P. *Angew. Chem., Int. Ed.* **2002**, *41*, 2578.
(20) Yan, H.; Beatty, A. M.; Fehlner, T. P. *J. Organomet. Chem.* **2003**, *680*, 66.
(21) Yan, H.; Beatty, A. M.; Fehlner, T. P. *J. Am. Chem. Soc.* **2003**, *125*, 16367.
(22) Yan, H.; Noll, B. C.; Fehlner, T. P. *J. Am. Chem. Soc.* **2005**, *127*, 4831.
(23) Yan, H.; Beatty, A. M.; Fehlner, T. P. *Organometallics* **2002**, *21*, 5029.
(24) Lei, X.; Shang, M.; Fehlner, T. P. *Chem. Eur. J.* **2000**, *6*, 2653.
(25) Macías, R.; Fehlner, T. P.; Beatty, A. M.; Noll, B. *Organometallics* **2004**, *23*, 5994.
(26) de Montigny, F.; Macias, R.; Noll, B.; Fehlner, T. P. *Angew. Chem., Int. Ed.* **2006**, *45*, 2119.
(27) Lei, X.; Bandyopadhyay, A. K.; Shang, M.; Fehlner, T. P. *Organometallics* **1999**, *18*, 2294.
(28) Macías, R.; Fehlner, T. P.; Beatty, A. M. *Angew. Chem., Int. Ed.* **2002**, *41*, 3860.
(29) Zimmerman, G. J.; Sneddon, L. G. *Inorg. Chem.* **1980**, *19*, 3650.
(30) Micciche, R. P.; Briguglio, J. J.; Sneddon, L. G. *Organometallics* **1984**, *3*, 1396.
(31) Wrackmeyer, B.; Schanz, H.-J.; Hofmann, M.; Schleyer, P.; Boese, R. *Eur. J. Inorg. Chem.* **1999**, 533.
(32) Wade, K. *Inorg. Nucl. Chem. Lett.* **1972**, *8*, 559.
(33) Wade, K. *Adv. Inorg. Chem. Radiochem.* **1976**, *18*, 1.
(34) Mingos, D. M. P. *Nature (London), Phys. Sci.* **1972**, *236*, 99.
(35) Mingos, D. M. P.; Wales, D. J. *Introduction to Cluster Chemistry*; Prentice Hall: New York, 1990.
(36) Williams, R. E. In *The Borane, Carborane, Carbocation Continuum*; Casanova, J., Ed.; Wiley-Interscience: New York, 1997; p 3.

Scheme 1

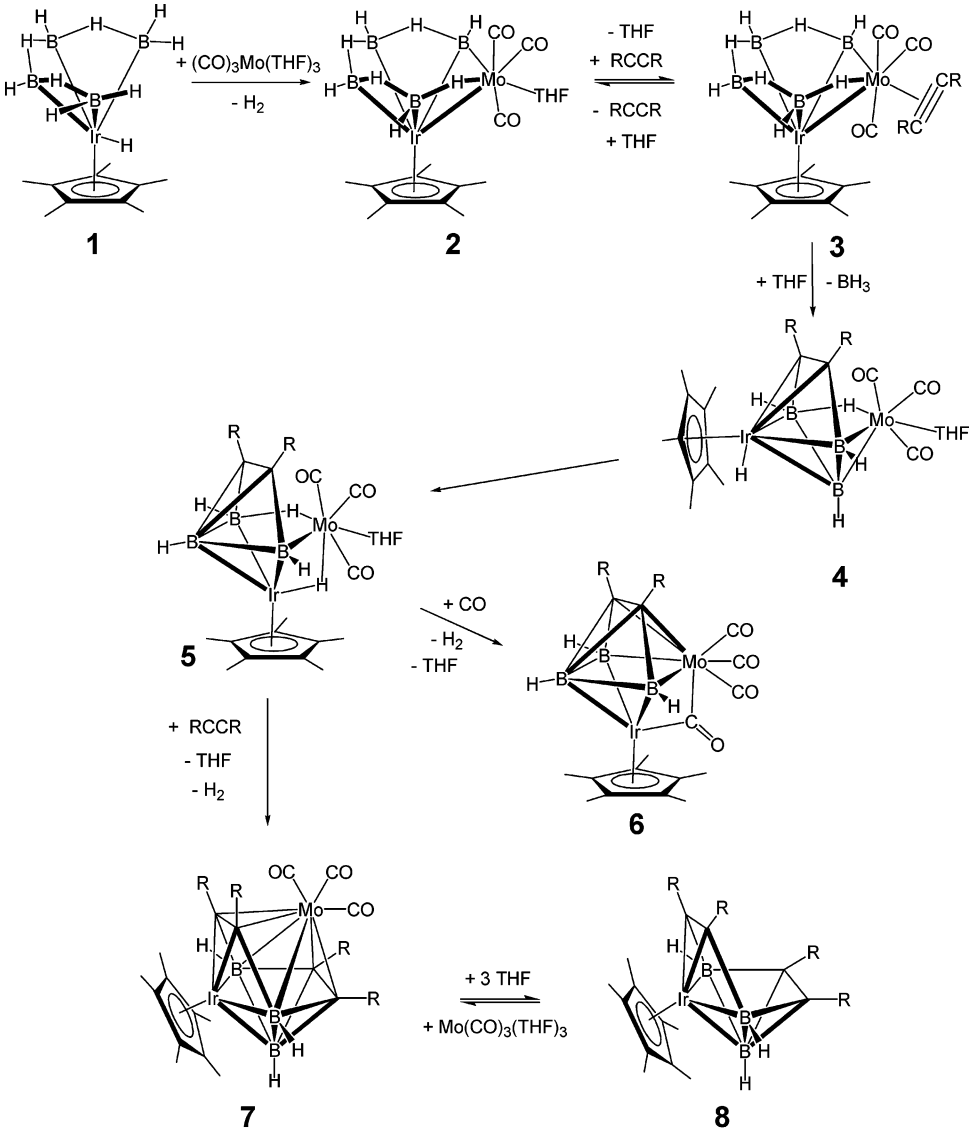

$$Cp^*IrB_4H_{10} + 2\ RCCR = Cp^*IrB_3H_3C_4R_4 + BH_3 + 2\ H_2:\ R = Me, Ph$$

As **8** reversibly coordinates to a Mo center (see below), the C−C distances of **8** are of interest. That for the C_2 unit not bonded to Ir in **8** is similar to that in its cobaltacarborane analogue (1.379(5) Å) as well as those in the isolobal main group analogue, $C_4Et_4B_4H_4$ (1.380(3) and 1.385(3) Å). That of the C_2 unit bound to Ir is slightly longer. As the angles around the carbon atoms in these clusters approach 120°, the skeletal carbons have sp^2 character similar to that of the C−C interaction in *nido*-2,3-$C_2B_4H_8$ and the B−B interaction in B_6H_{10}. Both of the latter compounds exhibit Lewis basicity, and cluster **8** is expected to do so as well. This conclusion is useful in explaining the reversible coordination of **8** to Mo described below.

With limited alkyne the same reaction generated a small yield of a different compound **6** in addition to **8**. Addition of alkyne to pure **6** under similar reaction conditions did not generate **8**; hence, **6** is a "dead-end" intermediate. Nonetheless, the NMR data for **6** are closely related to those of **8**, R = Me. There are two exceptions: the Me resonance integrates to 6 protons rather than 12, and the infrared spectrum shows metal CO bands including one absorption frequency consistent with a bridging carbonyl ligand. The spectrometric data suggest a composition $Cp^*IrMo(CO)_4B_3H_3C_2R_2$ with 8 sep. A closo seven-atom cluster containing Mo and Ir is predicted, and the solid-state structure in Figure 2 shows this to be the case. The observed geometric isomer, [1-Cp*-2,2,2-$(CO)_3$(μ-CO)-3,4-$(CH_3)_2$-*closo*-1,2,3,4-$IrMoC_2B_3H_3$], **6**, possesses a plane of symmetry containing B(2), Mo, and Ir. The carbon atoms are adjacent in the equatorial ring and Mo and B atoms occupy the apical positions. One of the four CO ligands bridges the Mo−Ir edge between the Mo-$(CO)_3$ and Cp*Ir fragments. For comparison with **8**, note that the C−C distance in **6** is considerably longer at 1.508 Å.

Penultimate Product. When the reaction mixture for R = Me was analyzed by NMR before workup, we were surprised to find that the signals due to **8** constituted a small fraction of the total intensity observed even though reactant **2** had been consumed. The major product was another species that had a

(37) King, R. B. *Inorg. Chem.* **2001**, *40*, 6369.
(38) Mavunkal, I. J.; Noll, B. C.; Meijboom, R.; Muller, A. Fehlner, T. P. *Organometallics* **2006**, *25*, 2906.

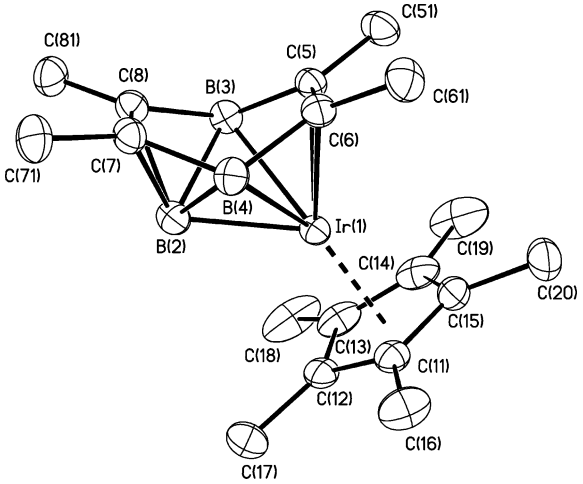

Figure 1. Molecular structure of [1-Cp*-5,6,7,8-(R)$_4$-*nido*-1,5,6,7,8-$IrC_4B_3H_3$], **8**, R = Me. Selected bond lengths [angstrom] and interatomic angles [deg]: Ir1−B2 2.089(2), Ir1−B3 2.305(2), Ir1−B4 2.289(2), Ir1−C5 2.1619(19), Ir1−C6 2.1619(19), B2−B3 1.953(3), B2−B4 1.943(3), C5−B3 1.572(3), C8−B3 1.603(3), C7−B4 1.600(3), C6−B4 1.577(3), C5−C6 1.414(3), C7−C8 1.384(3), C5−B3−C8 113.13(17), C7−B4−C6 113.04(18), B3−C5−C51 121.51(18), B3−C5−C6 115.64(17), C51−C5−C6 122.84(18), C51−C5−Ir1 123.64(14), B3−C8−C81 120.95(17), B3−C8−C7 115.30(17), C81−C8−C7 123.62(19), C81−C8−B2 129.14(19).

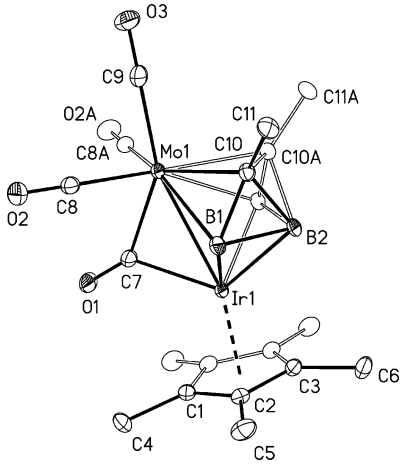

Figure 2. Molecular structure of [1-Cp*-2,2,2-(CO)$_3$(μ-CO)-3,4-(CH$_3$)$_2$-*closo*-1,2,3,4-$IrMoC_2B_3H_3$], **6**. Selected bond lengths [angstrom]: Ir(1)−C(7) 2.138(3), Ir(1)−B(1) 2.146(2), Ir(1)−B(2) 2.214(3), Ir(1)−Mo(1) 2.8751(6), Mo(1)−C(7) 2.152(3), Mo(1)−C(10) 2.3185(17), Mo(1)−B(1) 2.461(2), O(1)−C(7) 1.183(3).

spectroscopic signature similar to that of **8** but one that retained the molybdenum carbonyl fragment of **2**. The spectroscopic characterization of mixtures of the new product with **8** was consistent with a composition Cp*$IrB_3H_3C_4R_4Mo(CO)_3$, **7**. This cluster possesses 10 sep if the $Mo(CO)_3$ fragment is counted as a zero-electron fragment. Hence, with nine cluster fragments the counting rules suggest a closo geometry.

All initial attempts to isolate pure **7** by chromatography for a structure determination resulted solely in the isolation of **8**. Reactivity of **7** observed by NMR provided the key to solving the problem. Addition of PPh_3, toluene, or CH_3CN resulted in the loss of **7** and the formation of **8**. On the other hand, addition of excess (arene)$Mo(CO)_3$ resulted in the nearly quantitative formation of **7**. It was from the latter reaction mixture that single crystals of **7** were finally obtained.

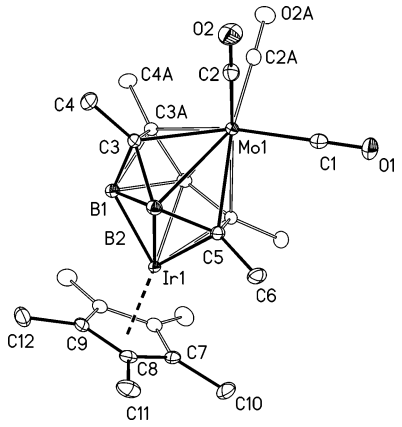

Figure 3. Molecular structure of [1-Cp*-5,6,7,8-(CH$_3$)$_4$-*closo*-1,5,6,7,8-$IrC_4B_3H_3Mo(CO)_3$], **7**. Selected bond lengths [angstrom] and interatomic angles [deg]: Ir(1)−B(1) 2.053(2), Ir(1)−C(5) 2.1433(13), Ir(1)−B(2) 2.3077(16), Mo(1)−C(3) 2.2355(13), Mo(1)−C(5) 2.3884(13), Mo(1)−B(2) 2.5716(16), Mo(1)−C(1) 1.999(2), Mo(1)−C(2) 1.9525(15), O(1)−C(1) 1.149(3), O(2)−C(2) 1.1603(18), C(5)−C(5) 1.448(3), C(3)−C(3) 1.451-(3), B(1)−C(3) 1.722(2), B(1)−B(2) 1.974(2), B(2)−C(5) 1.613(2), B(2)−C(3) 1.641(2), B(1)−B(2) 1.974(2), B(1)−Ir(1)−C(5) 86.23(7), C(5)−Ir(1)−C(5) 39.47(7), B(1)−Ir(1)−C(9) 99.62(7), B(1)−Ir(1)−B(2) 53.45(6), C(3)−B(1)−C(3) 49.83(11), C(3)−B(1)−B(2) 89.02(11), B(2)−B(1)−B(2) 90.05(13), C(3)−C(3)−C(4) 122.18(8), C(3)−C(3)−B(2) 114.12(7), C(5)−C(5)−C(6) 123.04(8), C(5)−C(5)−B(2) 114.64(7), C(6)−C(5)−B(2) 122.11-(12).

Scheme 2

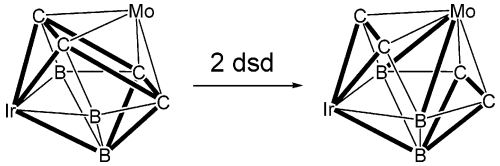

The solid-state structure of **7** is shown in Figure 3 and Scheme 1, where it can be seen that [1-Cp*-5,6,7,8-(CH$_3$)$_4$-*closo*-1,5,6,7,8-$IrC_4B_3H_3Mo(CO)_3$], **7**, is indeed closely related to **8**—a $Mo(CO)_3$ fragment has simply been added to the open face of **8**. As expected from the sep count, this is a closo cluster but is only so provided the Mo−B distance of 2.572(2) Å is considered bonding (more about this point below). If considered fully closed, the cluster geometry exhibited is not the canonical tricapped trigonal prismatic shape of the $[B_9H_9]^{2-}$ borane paradigm but rather a shape derived from it by two diamond−square−diamond rearrangements (Scheme 2). The six-connect vertex thereby generated is occupied by the Mo atom.

Considering the easily reversed formation of **7** from **8**, the iridatetracarbon−metallacarborane is usefully viewed as a complex ligand that can displace the six-electron arene in (arene)$Mo(CO)_3$ or, as the arene is probably largely lost in THF, the three THF ligands of $Mo(THF)_3(CO)_3$. The residual unsaturation of the C−C interactions in **8** mentioned above now becomes relevant. The C−C distances in **8** (1.38 and 1.41 Å) increase to 1.45 Å on binding the $Mo(CO)_3$ fragment to give **7**. Compare this to the C−C distance of 1.51 Å in **6** where the alkyne is strongly retained in the cluster network. There is a small increase of shielding of the alkyne carbons of **7** (δ 133.5, 133.4 ppm) on coordination to the Mo center (δ 129.6, 129.7 ppm). If the two "enes" are exclusive donors to the Mo atom then we have a formal 16-electron Mo complex. Hence, the Mo−B interaction is important in determining how to view coordination of **8** to Mo. The ^{11}B NMR shift change on

coordination of **8** is −10.4 to −10.6 for the two B atoms bonded to Mo, whereas it changes from 11.6 to 33.1 for the one B atom that is not. This is not helpful.

Quantum Chemical Analysis. Neither the structural metrics nor the spectroscopic shifts on coordination are definitive concerning the nature of the Mo−B interaction in **7**. If bonding, **7** is properly described as a closo cluster and can be viewed as an unusual cluster coordination compound with an 18-electron Mo center. If nonbonding, it would be described as a hypoelectronic open cluster and a cluster coordination compound with a 16-electron Mo center.[39] The nature of the Mo−B bonding must be addressed if one is to understand why the iridacarborane **8** is so weakly bound to the Mo fragment in **7**. Hence, **7**, as well as **6** and **8** for comparison, were investigated by quantitative quantum chemical methods at the density functional theory (DFT) level (see Computational Details). Models [1-Cp-2,2,2-$(CO)_3$(μ-CO)-3,4-$(CH_3)_2$-*closo*-1,2,3,4-$IrMoC_2B_3H_3$] (**6′**), [1-Cp-5,6,7,8-$(CH_3)_4$-*closo*-1,5,6,7,8-$IrC_4B_3H_3$-$Mo(CO)_3$] (**7′**), and [1-Cp*-5,6,7,8-$(R)_4$-*nido*-1,5,6,7,8-$IrC_4B_3H_3$] (**8′**) in which the Cp* ligand was replaced by Cp were used in order to reduce computational effort. These models were first optimized and compared to X-ray structures previously described (Cartesian coordinates of the optimized geometries are given in the Supporting Information).

Model **8′** within C_s symmetry, i.e., with the Cp and B_3C_2 (B(2)B(3)B(4)C(5)C(6)) rings eclipsed, is computed to be nearly isoenergetic (0.3 kJ/mol more stable) to the structure where the Cp and the B_3C_2 rings are slightly staggered with a torsion angle of 14°, close to that observed experimentally in **8** (12°). This slight staggering is probably due to weak steric hindrance between the Me groups of Cp* and the R groups attached to the carbon atom of the B_3C_2 ring. The metrical data computed for **8′** are in good agreement with those experimentally measured for **8**. The largest bond distance and bond angle deviations are 0.02 Å and 2°, respectively. A good agreement between theory and experiment is also observed between **6** and **6′**. The main discrepancy is for the Mo−C(5) bond (see Figure 2 for atom labeling), which is computed to be 0.04 Å longer than that measured experimentally. Model **7′** also quite satisfactorily mimics the arrangement of the crystallographically characterized cluster **7** with a slight overestimation of the Mo−C and Mo−B distances (0.03−0.05 Å for Mo−C, 0.03 Å for Mo−B).

The long Mo−B separations, which we seek to interpret, are well reproduced in **7′** (2.602 vs 2.572 Å experimental) and the normal separations are also reproduced in **6′** (2.459 vs 2.461 Å experimental). Do the calculations also show a difference in the $Mo(CO)_3$–cluster binding energies? Investigation of these interactions utilizes an energy-partitioning analysis.[40,41] This approach allows one to estimate the interaction energy (ΔE_{int}) between the two fragments as the sum of the energy contributions of the stabilizing orbital interactions (ΔE_{orb}) and the steric interaction (ΔE_{ste}), which is the sum of the attractive electrostatic contributions (ΔE_{elst}) and the Pauli repulsions (ΔE_{Pauli}). ΔE_{int} between the fragments $Mo(CO)_3$ and [1-Cp-5,6,7,8-$(Me)_4$-*nido*-1,5,6,7,8-$IrC_4B_3H_3$] is −3.16 eV (305 kJ/mol), mainly due to attractive orbital interactions (ΔE_{orb} = −5.88 eV and ΔE_{ste} = 2.72 eV). A similar fragmentation for **6′**, i.e., $Mo(CO)_3$ and Cp-

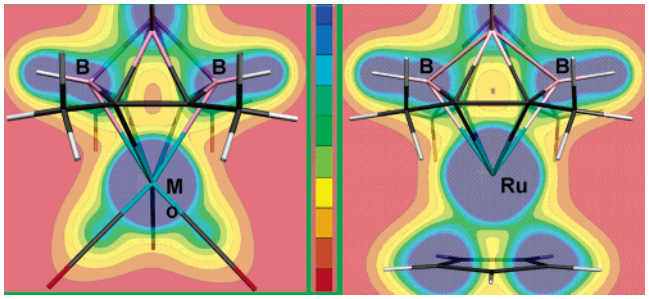

Figure 4. Total electron density plots in the metal−B−B plane for (a) **7′** and (b) [1-Cp-5,6,7,8-$(CH_3)_4$-*closo*-1,5,6,7,8-$IrC_4B_3H_3RuCp]^+$. Contour plots range from 0.0 (red) to 0.13 *e*/bohr^3 (blue).

(CO)$IrC_2Me_4B_3H_3$, gives an interaction energy of −5.81 eV, which results from ΔE_{orb} = −10.25 eV and ΔE_{ste} = 4.45 eV. Consistent with the experimental observations, these results show that the Mo−cluster binding is considerably stronger in the case of **6′** than **7′**.

Is the difference in binding energies caused by lack of Mo−B interactions in **7′**, i.e., is **7** best described as a 16-electron Mo cluster complex or, alternatively, a hypoelectronic metallacarborane? This is a much more difficult question to answer but can be addressed by partitioning the electronic structure solution with methods previously found useful. Partitioning of the binding energies of **6′** and **7′** is problematical as the two Mo−cage interactions are significantly different in the two cases. That is, **6′** has a Mo−Ir bridging carbonyl, as well as a Mo−Ir bond, and its larger binding energy does not necessarily mean the Mo−B binding is weak in **7′**.

For this reason the nature of the Mo−B bonds in **7′** was examined by analyzing the electron density distribution. A cut corresponding to the Mo−B−B plane is shown in Figure 4. The density in this region is small and supports a weak Mo−B interaction at best. A frontier molecular orbital (FMO) fragment analysis of the MO diagram of **7′** is consistent with this conclusion. The FMOs of the $Mo(CO)_3$ moiety (a typical ML_3 fragment with three hybrids FMOs of σ and π type above three occupied "t_{2g}" FMOs) mainly interact with FMOs of the cluster which have a carbon character. Indeed, only two MOs of **7′** with a tiny Mo−B bonding character can be identified at low energy (HOMO-6 and HOMO-9), leading to a very weak Mo−B interaction.

The "synthesis" of a late metal derivative was carried out for comparison, i.e., the $Mo(CO)_3$ fragment was replaced with an isolobal $[RuCp]^+$ fragment as this particular fragment is experimentally accessible via $[Cp^*Ru(NCCH_3)_3][PF_6]$.[42] This hypothetical molecule has an optimized geometry similar to that of **7′** and a computed binding energy 2 eV higher (5.12 eV vs 3.16 for Mo)! The HOMO−LUMO gap also increases significantly in going from **7′** to the $[RuCp]^+$ analog (1.3−1.8 eV). These results led to several attempts to synthesize the ruthenium derivative by the reaction of **8** with a source of the $[RuCp^*]^+$ fragment. Unfortunately, none were successful, but the molecule should be able to be isolated if an appropriate route can be discovered.

A possible explanation for the larger binding energy between the ruthenium entity and the cluster might be that the $[RuCp]^+$ fragment interacts with the four carbon atoms *and* the two boron

(39) Ghosh, S.; Beatty, A. M.; Fehlner, T. P. *Angew. Chem., Int. Ed.* **2003**, *42*, 4678.
(40) Morokuma, K. *J. Chem. Phys.* **1971**, *55*, 1236−1244.
(41) Ziegler, T.; Rauk, A. *Theor. Chim. Acta* **1977**, *46*, 1−10.
(42) Francis, M. D.; Holtel, C.; Jones, C.; Rose, R. P. *Organometallics* **2005**, *24*, 4216.

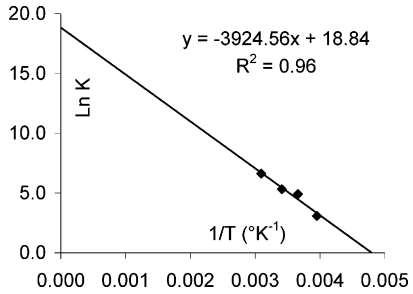

Figure 5. Plot of ln K' vs $1/T$ derived from ^{11}B NMR intensities signals from 7 and 8 in equilibrium 1.

atoms, whereas the $Mo(CO)_3$ moiety interacts only with four carbon atoms in **7′**. To check this hypothesis, the total electron density between B and the metal for **7′** was compared with that in the $[RuCp]^+$ analog (Figure 4). The magnitude of the density in the latter is also consistent with a weak Ru−B interaction only slightly more important than in **7′** at best. In essence, the binding in the $[RuCp]^+$ derivative is similar to that in **7′**, i.e., Mo−cluster interactions are mainly via M−C contacts, which are somewhat stronger because of better orbital interactions between the FMOs of the $[RuCp]^+$ and the iridacarborane cluster.

All our analyses of the results suggest that the Mo−B interaction in **7′** is weak and the binding to Mo resides largely in the Mo−C interactions. We conclude that **7** is appropriately viewed as a 16-electron cluster Mo coordination compound where cluster **8** acts as a four-electron donor. Certainly it may also be viewed as a single hypoelectronic cluster containing two transition metals; however, this is much less informative. The solution is pleasing as it accommodates the experimentally observed weak binding of cluster **8** to the Mo center and its ready displacement by Lewis bases. Both are of crucial importance to the ultimate release of the final product **8** by base displacement.

Equilibrium Constant. The observation that the ratio **7** to **8** in a mixture of the two compounds can be increased by the addition of (arene)$Mo(CO)_3$ and decreased by the addition of a Lewis base suggests the existence of equilibrium 1. As equilibrium properties provide access to important thermodynamic parameters, the equilibrium constant, K_{eq}, was measured. Equilibrium mixtures were prepared by adding measured amounts of (arene)$Mo(CO)_3$ and **8** to a known volume of THF. The NMR tube containing the mixture was heated at 50 °C to form **7** and then equilibrated at a chosen temperature for up to 16 h at the lowest temperature. The equilibrium ratio of **7** to **8** was measured by ^{11}B NMR at the temperatures, −20, 0, 20, and 50 °C. Equilibrium 1 written as a formation reaction for **7**

$$\mathbf{8} + Mo(THF)_3(CO)_3 \rightleftarrows \mathbf{7} + 3THF; \quad K' = K_{eq}/[THF]^3 \quad (1)$$

is a slightly endothermic process, i.e., the mole fraction of **7** increases from 0.4 at −20 °C to 0.8 at 50 °C. As shown in Figure 5 straight line fit to a plot of ln K' versus $1/T$ gave ΔH = 8 kcal/mol and ΔS = 37 cal/mol K. These are approximate values because raw NMR intensities were used for concentration measurements, the presence of arene was ignored, and the temperature range was small. However, because of the exponential relationship between K_{eq} and free energy even a crude measure of the former gives useful energy values. Addition of (arene)$Mo(CO)_3$ to **8** (R = Ph) did not yield any measurable **7**

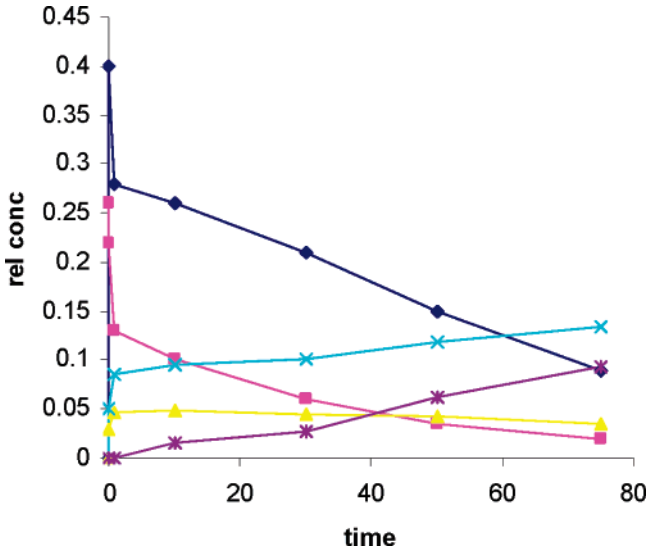

Figure 6. Plot of reaction time vs relative abundances of reactants and products based on ^{1}H NMR signal intensities (2-butyne, dark blue diamonds; **2**, magenta squares; **7**, brown double crosses; **5**, azure crosses; **4**, yellow triangles).

(R = Ph). Either the reaction has a substantially higher barrier or the greater steric bulk of Ph versus Me decreases K' sufficiently to reduce the concentration of **7** below the level of NMR detection.

As described above the gas-phase binding energy of a $Mo(CO)_3$ fragment to **8** (for Cp rather than Cp*) is exothermic by 3.16 eV. The 8 kcal/mol endothermicity of equilibrium 1 shows that the binding energy of three THF molecules to $Mo(CO)_3$ is larger than the binding energy of **8** to the Mo center. The large positive entropy change associated with equilibrium 1 is a result of the fact that two entities are converted into four which, in the gas phase, would constitute an increase of six translational degrees of freedom. The enthalpic and entropic factors largely balance each other at room temperature, and the equilibrium constant is sufficiently close to unity to permit both **7** and **8** to be observed in the equilibrium mixture at room temperature.

We conclude that, as cluster carbon content increases, the binding energy to the Mo center decreases mainly due to a loss of Mo−B bonding. As a consequence, the addition of two alkyne units leads to sufficiently poor binding that Mo is readily displaced by basic solvents or silica gel. The presence of the Mo center in **2** facilitates the addition of alkyne, but it is the change in Mo−cluster binding with carbon content that leads to the detachment of the Mo center. As a result, the overall process in Scheme 1 constitutes a classic example of a metal-facilitated transformation where the substrate is a metallaborane rather than an organic molecule.

Reaction Intermediates. In the first hour of the reaction of **2** with 2-butyne, two species, **4** and **5**, are observed by ^{1}H and ^{11}B NMR to form before the fully characterized products **7** and **8** described above. (Product **6** is only abundant under conditions of alkyne deficiency described above.) A plot of NMR signal intensities of these species as a function of time relative to those of the isolated products is shown in Figure 6. The shapes of the curves are consistent with **4** and **5** arising from **2** and leading to **7**. Although **4** and **5** appear in parallel, **5** is in higher abundance with a longer life time under the reaction conditions. Assuming the compositions and structures for **4** and **5** shown

Table 1. NMR Assignment of $IrB_3H_3C_4Me_4$ and Intermediates

		2	4	5	6	7
^{1}H NMR	Cp*	1.80 (15 H)	2.17 (15 H)	2.06 (15 H)	1.54 (15 H)	1.92 (15 H)
	BH_t	7.0 (1 H) 3.6 (1 H) 3.4 (1 H) 3.1 (1 H)	5.20 (2 H) 2.43 (1 H)	5.16 (2 H) 3.01 (1 H)	5.48 (2 H) 2.77 (1 H)	5.36 (1 H) 1.54 (2 H)
	Me		2.0 (6 H)[a]	2.1 (6 H)	2.24 (6 H)	2.44 (6 H) 2.10 (6 H)
	H−B−M	0.3 (1 H) −3.1 (1 H) −3.5 (1 H)	−5.2	−5.0 (1H)		
	H−M	−6.9 (1 H)	−11.51(1 H)	−20.47(1 H)		
^{11}B NMR		44.7 (1 B) 9.5 (1 B) −5.0 (1 B)	32.5 (2 B) 1.1 (1 B)	33.9 (2 B) −6.1 (1 B)	33.4 (2 B) 1.9 (1 B)	33.1 (1 B) 1.1 (2 B)

[a] Assignment uncertain.

in Scheme 1 (assignments discussed below), the overall mass balance is good suggesting there are no more intermediate products of comparable abundance. An important consequence is that the mass balance is only good for the Me resonances if **4** and **5** each contain one alkyne moiety. At a reaction time where the system contains only **5** and **7** (plus a small amount of **8**), addition of excess alkyne converts **5** to **7** quantitatively by ^{11}B NMR (see Figure B, Supporting Information).

The structural assignments for **4** and **5** are based on the known spectroscopic and structural data of the reactant **2** and products **7** and **8**. The time dependence of the signals provides a low-resolution marker that allows the complex Me and Cp* region of the ^{1}H NMR to be sorted and assigned. Although the broad ^{11}B NMR signals showed the same trends in composition with time (Supporting Information, Figure B), it was the well-resolved ^{1}H data that provided the data for Figure 6.

The NMR assignments of **4** and **5** are given in Table 1, where it will be seen that the two intermediates are closely related to each other as well as to **2** and **7**. The Me resonance associated with **4** is tentative, and the mass balance above is a stronger argument for the presence of one alkyne moiety in this intermediate. In addition, the individual assignments of the B−H terminal resonances to **4** versus **5** could be interchanged. On the other hand, confidence in the assignments of the high-field hydrides and Cp* resonances is high as they are well resolved and there is a time period when **5** and **7** are the predominant species present. The following summarizes the reasoning leading to the proposed structures of **4** and **5** shown in Scheme 1.

With single alkyne residues **4** and **5** are reasonable precursors to **7** by addition of alkyne and **6** by loss of H_2 (and THF/CO exchange). Further, like **6** and **7** the two intermediates contain three B−H fragments; hence, a B−H fragment must be lost in a relatively rapid step in going from **2** to the intermediates. The total number of high-field hydride signals associated with **6** and **7** require the loss of 2 H as well; hence, in going from **2** to the intermediates 1 mol of alkyne is added and the elements of BH_3 are lost. The latter has been well documented previously in the reactions of alkynes with *nido*-$(Cp^*RuH)_2B_3H_7$.[20−22] At this point we have a composition $Cp^*IrB_3H_5C_2R_2$, but a Mo fragment is almost certainly present. If it is a $Mo(CO)_3$ fragment the species would have 8 sep and a probable closo structure like **6**. This is unlikely as **6**, like closed clusters in general, is a stable end product. For this reason, as well as the fact that another alkyne must be added to reach **7**, we suggest retention of the $Mo(CO)_3THF$ fragment of **2** in **4** and **5**. This give a 9 sep count and a nido structure for each.

The formulation of both **4** and **5** as *nido*-$Cp^*IrB_3H_5C_2R_2$-$Mo(CO)_3THF$ requires that they be isomers. It is reasonable to assume that $Cp^*IrB_3H_3$ and the R_2C_2 fragments observed in **6**−**8** remain intact in **4** and **5**. Thus, the difference between **4** and **5** is the relative positions of the Ir and Mo metals. The Ir and Mo atoms are adjacent in **2** and **6** and should be so placed in either **4** or **5**. For reasons discussed next the structures are assigned as [1-Cp*-7,7,7-$(CO)_3$-7-THF-2,3-$(CH_3)_2$-*nido*-1,7,2,3-IrMo$C_2B_3H_5$], **4**, and [5-Cp*-7,7,7-$(CO)_3$-7-THF-2,3-$(CH_3)_2$-*nido*-5,7,2,3-Ir$MoC_2B_3H_5$], **5**, and shown in Scheme 1.

In a mechanistic context, two roles for **4** and **5** are possible: a consecutive path of **2** to **4** to **5** to **7** or a parallel path **2** to **4**, **5** to **7**. Unfortunately, as already mentioned, the early time resolution of the NMR signal intensities does not permit the two to be distinguished. In the absence of definitive information we have used a consecutive pathway in Scheme 1 as it is a more satisfying one. Considering the position of the labile THF ligand in **2**, it is reasonable that alkyne insertion takes place via the Ir−Mo edge. If so, elimination of BH_3 from an intermediate not shown leads to **4** with nonadjacent metals. Rearrangement to **5** with adjacent metals permits insertion of another alkyne or, if alkyne is limiting, unimolecular H_2 elimination and formation of **6**. Note that the ^{11}B resonance of the unique boron shifts upfield smoothly in going from **4** (1.1 ppm) to **5** (−6.1 ppm) to **7** (−10.6 ppm) consistent with position connectivities and nearest neighbor atom identities.

Although the structures of **4** and **5** cannot be viewed as definitive, the overall mechanistic picture is clear—sequential addition of alkyne competitive with BH_3 or H_2 fragment elimination. This stoichiometric process is fully consistent with earlier cluster mechanistic information in the literature.[43]

Olefin Isomerization—Mechanistic Probe. What remains to be defined is the initial step in going from **2** to **4**. Circumstantial evidence implicates dissociation of the labile THF and coordination of the alkyne to Mo as prerequisite to the insertion process. If alkynes coordinate to **2**, then olefins should also displace THF from **2**. However, in contrast to

(43) Shriver, D. F., Kaesz, H. D., Adams, R. D., Eds. *The Chemistry of Metal Cluster Complexes*; VCH: New York, 1990.

Scheme 3

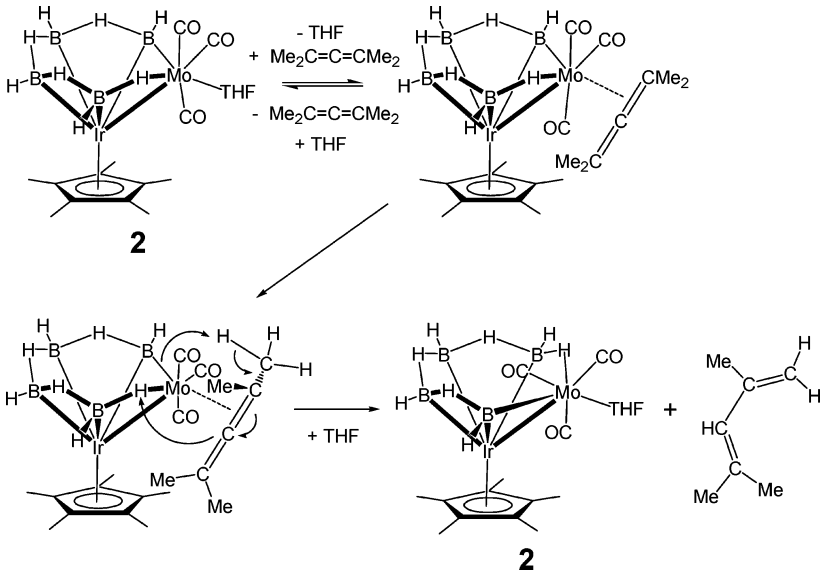

alkynes, olefins have not been found to yield metal−boron-containing products under mild conditions for any members of this class of metallaboranes. Although a disappointment in terms of new derivatives, this negative observation provides a way of probing the coordination process. Thus, we now show that two olefins, tetramethylallene and hexane, provide evidence of THF displacement and coordination to **2**. This supports reversible binding of alkyne to the Mo site of **2** to form **3** as shown in Scheme 1. As the results on hexene serve as a foundation for understanding the allene reaction, they are presented first.

The reaction of hex-1-ene with 1 mol % of **2** leads to the slow generation of *cis*-hex-2-ene with a turnover rate averaging 6/day (Table A, Supporting Information). If light is excluded, no *trans*-hex-2-ene is observed. Unfortunately, **2** degrades to unknown, intractable products on roughly the same time scale as the catalytic reaction, but by replacing it daily a total conversion of 96% is achieved in 10 days (2.3 mmol hex-2-ene produced with a total of 0.43 mmol **2** added). Continued addition of catalyst led to a final conversion of 98%. Examination of the reverse reaction with hex-2-ene containing approximately 1% hex-1-ene impurity showed no reaction. Note that thermal isomerization of hex-1-ene requires more vigorous conditions.[44,45]

The catalytic isomerization of olefins is well studied, and the general features of the mechanism are understood.[9] Hence, our observations can be used to comment on the nature of **2** provided decomposition products can be excluded as the active catalyst. The isomerization of pen-1-ene to a mixture of both *cis*- and *trans*-pen-2-ene by ruthenium carbonyl clusters has been reported.[46] Such clusters are more prone to metal loss than metallaboranes. This contrasts with the sole conversion to the cis isomer here and, along with the observations on the allene below, suggests that the decomposition products of **2** are not significantly active.

The general mechanism for known mononuclear catalysts consists of addition of the olefin to a vacant site, H transfer to the metal with formation of an allyl complex, H transfer back to the ligand, and generation of either the original alkene or its isomer. For the metallaborane we suggest that the olefin displaces THF from **2**, undergoes rearrangement at the Mo site, and is displaced by THF, i.e., for the alkene, step **2** to **3** in Scheme 1 takes place but the insertion pathway available to the alkyne does not. In contrast, the addition of a B−H bond to an olefin takes place in an anti-Markownikoff sense, and although hydroboration of alkynes was observed for a ruthenaborane,[22] the B−H bonds of **2** do not react with either alkene or alkyne.

When tetramethylallene is added to a solution containing **2** there is an instant color change which we attribute to formation of a complex, i.e., the binding constant for the allene is larger than that of the hexene. Once again no reaction is observed other than the conversion of the cumulene to an isoprene derivative (2,4-dimethylpenta-1,3-diene) as shown in eq 2. On the basis of the ^{1}H and ^{13}C NMR the TON after 3 h were 18 and 11, respectively, at 50 °C and 6.5 at room temperature. Conversions ranged from 7% to 20%. The room-temperature catalytic rate (2 turnovers/h) is about 1 order of magnitude larger than that found for hexene (0.25 turnovers/h), which is consistent with the apparently higher binding constant mentioned above.

$$Me_2C{=}C{=}Me_2 \rightarrow \textit{cis}\text{-}H_2C{=}C(Me)CH{=}C(Me)_2 \quad (2)$$

In the absence of a catalyst, tetramethylallene dimerizes quantitatively to tetramethyl-1,2-di-isopropylidenecyclobutane without isomerization in 72 h at 150 °C in a reaction vessel pretreated with strong base.[44] The isomerization reaction 2 as well as more complex dimerization occurs on proton acidic surfaces in 24 h at the same temperature.[44] In a cluster, it is the bridging hydrogen atoms that are most acidic, and in a metallaborane such as **2**, the Mo−H−B hydrogen is expected to be more acidic than B−H−B hydrogen. The former, being adjacent to the Mo binding site, is readily available for transfer to a bound allene. Further, the other Mo−B edge of **2** lacks a bridging hydrogen atom and is available to accept a proton. Hence, the mechanism sketched in Scheme 3, where the arrows show movement of electron density, is a viable one for the

(44) Taylor, D. R.; Wright, D. B. *Chem. Commun.* **1968**, 434.
(45) Taylor, D. R.; Wright, D. B. *J. Chem. Soc. B* **1971**, 391.
(46) Gladfelter, W. L.; Roesselet, K. J. In *The Chemistry of Metal Cluster Complexes*; Shriver, D. F., Kaesz, H. D., Adams, R. D., Eds.; VCH: New York, 1990; p 329.

observed isomerization at room temperature. In essence, coordination of one double bond is followed by transfer of a methyl proton to the Mo−B edge as the Mo−H−B proton is transferred to the central allenic carbon atom. Release of the less strongly bound 1,3-diene (see hexene results) completes the isomerization.

These observations are consistent with those on hexene and establish step 2 to 3 in the mechanism of Scheme 1, i.e., the intermediate is [1-Cp*-2,2,2-$(CO)_3$-2-(alkyne)-*nido*-1,2-IrMo-B_4H_8], **3**. Thus we have built up a stoichiometric mechanism for the complex overall reaction. It does mimic a typical metal-facilitated reaction in organometallic chemistry. That is, step 1 to 2 constitutes metal incorporation into the iridaborane substrate. Step 2 to 3 describes the Mo-facilitated assembly of the second substrate. Step 3 to 4 denotes reaction of the alkyne and iridaborane substrates which, in this case, is alkyne insertion into the cluster framework. Steps 4 to 5 and 5 to 7 describe the incorporation of the second alkyne with concomitant decrease in the strength of the association of the Mo center with the original iridaborane framework. Equilibrium 7 to 8 constitutes product release and reformation of the Mo complex originally used to generate **2** from **1**.

Conclusions

A comparison of the reactivities of ruthena-, rhoda-, and iridaboranes with alkynes further resolves the structural factors that define the productive interaction with alkynes under mild conditions. The first factor of importance is cluster geometry/electron count. Earlier work showed that isoelectronic *nido*-ruthena- and rhodaborane clusters easily add alkyne giving arachno cluster intermediates. This leads to exclusively to cyclotrimerization for the rhodaborane and predominantly to ruthenacarboranes for the ruthenaborane. Although alkyne addition is facile for both metallaboranes, only in the case of ruthenium are there additional cluster hydrogen atoms to facilitate hydrometallation of the alkyne and initiate the formation of a variety of novel derivatives containing the alkyne components.

In the synthesis of the group 9 metallaborane congeners from monoborane and monocyclopentadienyl metal chlorides, the cobalt and rhodium derivatives evolve H_2 until nido clusters are isolated, whereas for iridium the process stops at the electron-rich arachno products. Hence, although the *arachno*-iridaborane has an abundance of hydrogen atoms, Lewis base addition is not favored. The tendency to lose a pair of electrons is greater than that for addition. As a consequence, the iridaborane alone does not react with alkynes under mild conditions. Introduction of a metal center with a weakly coordinated THF molecule into the iridaborane cluster provides a nexus for alkyne coordination and leads to metallacarborane formation, albeit with interesting additional features. Because the added metal center binding decreases with added carbon content, it is easily removed, thereby completing the metal-facilitated process of alkyne addition to the iridaborane cluster.

The introduction of transition metal centers into a borane framework provides a variety of cluster analogues of boranes that often are easily understood with the cluster electron counting rules and isolobal ideas. That is, from a purely geometrical/structural viewpoint, the Ru, Rh, Ir clusters are routine. The comparative chemistry, outlined above, shows how deceptive such a view really is. For the same substrate, metal identity completely dominates the predominant reaction pathway observed. Metal choice, then, provides a way to control reactivity and suggests continued study of structurally similar but compositionally different metallaboranes will be profitable.

Experimental Section

General Considerations. All reactions were carried out under an argon atmosphere using standard Schlenk-line techniques.[47] Solvents were distilled immediately before use under a dinitrogen atmosphere: sodium benzophenone ketyl for hexanes and tetrahydrofuran and calcium hydride for dichloromethane. All commercial reagents were used as received without further purification. The iridapentaborane **1** and the (arene)tricarbonylmolybdenum complex were prepared by following synthetic procedures previously reported.[25,27,28] NMR spectra were recorded on a 400 MHz Bruker instrument. NMR references: internal (C_6D_6, δ_H 7.16 ppm) for ^{1}H; external ([$(Me_4N)(B_3H_9)$] in acetone-d_6 δ_B −29.7 ppm) for ^{11}B. IR spectra were recorded on a Nicolet 205 FT−IR spectrometer. Mass spectra were acquired on a Finnigan MAT model 8400 mass spectrometer. M-H-W Laboratories, Phoenix, AZ, performed the elemental analysis.

The heterometallaborane **2** was prepared and used in situ by adding *arachno*-[Cp*IrB_4H_{10}] (100 mg, 0.26 mmol) to Mo(tol)$(CO)_3$ (100 mg, 0.37 mmol) in freshly distilled THF (5 mL). This mixture was stirred at 50 °C for 10 min to generate **2**, and then a large excess of 2-butyne (0.1 mL, 1.28 mmol) was added. The reaction mixture was stirred 2 h. The mixture was purified by TLC (silica, hexane) to afford **8** (R = Me, 24 mg, 20%) and a trace of **6**. Yellow crystals of **8** were obtained from hexane. By a similar method, a 28% yield of **8**, R = Ph, was obtained, and yellow crystals were grown from CH_2Cl_2/hexane. Improved yields of **6** (4 mg, 2%) were obtained by using less than 1 equiv of 2-butyne (0.02 mL, 0.25 mmol). A mixture of **8** (R = Me, 10 mg, 0.02 mmol) and Mo(tol)$(CO)_3$ (10 mg, 0.04 mmol) in dry THF-d_6 (0.5 mL) was heated at 50 °C for 3 h at which point the ^{11}B NMR spectrum shows large conversion to **7**. Although some **8** was present, a few brown crystals of **7** were obtained from this solution at −20 °C.

[1-Cp*-5,6,7,8-$(CH_3)_4$-*nido*-1,5,6,7,8-$IrC_4B_3H_3$], 8, R = Me. ^{11}B NMR ([D_6]benzene, 22 °C, 128 MHz): δ = 11.6 (d, ^1J(H,B) = 157 Hz, 1B; BH), −10.4 (d, ^1J(H,B) = 128 Hz, 2B; BH). ^{1}H{^{11}B} NMR ([D_6]benzene, 22 °C, 400 MHz): δ = 5.16 (s, 1H; BH_t), 2.30 (s, 2H; BH_t), 2.19 (s, 6H; CH_3), 1.88 (s, 6H; CH_3), 1.68 (s, 15H; Cp*). ^{13}C-{^{1}H} NMR ([D_6]benzene, 22 °C, 100 MHz): δ = 133.5 (CCH_3), 133.4 (CCH_3), 92.9 ($C_5(CH_3)_5$), 22.7 (CH_3), 19.0 (CH_3), 9.3 ($C_5(CH_3)_5$). IR (KBr): 2956 (s), 2924 (s), 2855 (s), 2453 (s, B−H), 2019 (w), 1950 (w), 1929 (w), 1460 (m), 1379 (m), 1262 (m), 1091 (m), 1029 (m), 951 (w), 798 (s). LR-MS (FAB): *m*/*z* isotope envelope; 471 $[M]^+$, 3 B, 1 Ir atoms, calcd for weighted average of isotopomers ($C_{18}H_{30}B_3Ir$) lying within the instrument resolution 472.2256; obsd, 472.2258. Elemental analysis (%) calcd for $C_{18}H_{30}B_3Ir$: C, 45.89; H, 6.42. Found: C, 45.70; H, 6.60.

[1-Cp*-6,7,8,8-Ph_5-*nido*-1,6,7,8,8-$IrC_5B_4H_4$], 8, R = Ph. ^{11}B NMR ([D_6]benzene, 22 °C, 128 MHz): δ = 9.6 (d, ^1J(H,B) = 180 Hz, 1B; BH), −9.1 (d, ^1J(H,B) = 73 Hz, 2B; BH). ^{1}H{^{11}B} NMR ([D_6]benzene, 22 °C, 400 MHz): δ = 7.41 (d, ^3J(H,H) = 8 Hz, 4H, PhH), 7.35 (d, ^3J(H,H) = 8 Hz, 4H, PhH), 7.07 (t, ^3J(H,H) = 7 Hz, 4H, PhH), 7.01−6.95 (m, 8H, PhH), 5.53 (s, 1H; BH_t), 3.07 (s, 2H; BH_t), 1.60 (s, 15H; Cp*). ^{13}C{^{1}H} NMR ([D_6]benzene, 22 °C, 100 MHz): δ = 144.0 (PhC*i*), 143.6 (PhC*i*), 132.3 (PhC*o*), 127.3 (PhC*m*), 126.7 (PhC*p*), 94.8 ($C_5(CH_3)_5$), 9.9 ($C_5(CH_3)_5$). IR (hexane): 2497 (s, B−H), 2020 (s), 1954 (s), 1940 (w), 1599 (w), 1262 (s), 1099 (s), 1018 (s). LR-MS (FAB): *m*/*z* isotope envelope; 719 with cutoff at 720, $[M^+]$, 3 B, 1 Ir atoms, calcd for weighted average of isotopomers $C_{38}H_{38}B_3Ir$ lying within the instrument resolution 720.2882; obsd, 720.2873.

(47) Shriver, D. F.; Drezdzon, M. A. *The Manipulation of Air Sensitive Compounds*, 2nd ed.; Wiley-Interscience: New York, 1986.

[1-Cp*-2,2,2-(CO)$_3$(μ-CO)-3,4-(CH$_3$)$_2$-*closo*-1,2,3,4-IrMoC$_2$B$_3$H$_3$], 6. ^{11}B NMR ([D$_6$]benzene, 22 °C, 128 MHz): δ = 33.4 (d, ^1J(H,B) = 138 Hz, 2B; BH), 1.9 (d, ^1J(H,B) = 168 Hz, 1B; BH). ^{1}H{^{11}B} NMR ([D$_6$]benzene, 22 °C, 400 MHz): δ = 5.48 (s, 2H; BH$_t$), 2.77 (s, 1H; BH$_t$), 2.24 (s, 6H; CH$_3$), 1.54 (s, 15H; Cp*). IR (hexane): 2518 (w, B−H), 2137 (w, CO), 2022 (s, CO), 1997 (s, CO), 1925 (s, CO), 1936 (s, CO), 1820 (m, μ-CO), 1271 (m), 1102 (m), 1011 (m). LR-MS (FAB): *m*/*z* calcd for C$_{18}$H$_{24}$IrMoB$_3$O$_4$ isotope envelopes; 626, 19% [M$^+$], 598, 18% [M−CO$^+$], 569, 65% [M−(CO)$_2^+$], 513, 100% [M−CH$_3$C$_2$CH$_3$−(CO)$_2^+$].

[1-Cp*-5,6,7,8-(CH$_3$)$_4$-*closo*-1,5,6,7,8-IrC$_4$B$_3$H$_3$Mo(CO)$_3$], 7. ^{11}B NMR ([D$_8$]THF, 22 °C, 128 MHz): δ = 33.1 (d, ^1J(H,B) = 160 Hz, 1B; BH), −10.6 (d, ^1J(H,B) = 137 Hz, 2B; BH). ^{1}H{^{11}B} NMR ([D$_8$]-THF, 22 °C, 400 MHz): δ = 5.36 (s, 1H; BH$_t$), 2.44 (s, 6H; CH$_3$), 2.10 (s, 6H; CH$_3$), 1.92 (s, 15H; Cp*), 1.54 (s, 2H; BH$_t$). ^{13}C{^{1}H} NMR ([D$_8$]THF, 22 °C, 100 MHz): δ = 202.1 (CO), 129.6 (CMe), 129.5 (CMe), 92.9 (C$_5$(CH$_3$)$_5$), 21.5 (CH$_3$), 18.5 (CH$_3$), 9.3 (C$_5$(CH$_3$)$_5$). IR ([D$_8$]THF): 2495 (s, B−H), 1980 (w, CO), 1941 (w, CO), 1893 (m, CO), 1854 (m, CO). LR-MS (FAB): *m*/*z* isotope envelope; 471 [M]$^+$, 3 B, 1 Ir atoms corresponding to the fragment ion [Cp*IrC$_4$-(CH$_3$)$_4$B$_3$H$_3$]$^+$.

NMR Equilibrium Experiment. To obtain K' as a function of T, a mixture of **8** (31 mg, 0.066 mmol) and Mo(tol)(CO)$_3$ (15 mg, 0.055 mmol) in THF-d_8 was heated at 50 °C for 3 h in an NMR tube and then equilibrated at the temperature of choice. At 50 °C the composition was unchanged after another 3 h. At 20 and 0 °C measurements were taken after 5 h, whereas at −20 °C they were taken after 16 h. The mole fraction of **7** was determined by ^{11}B NMR to be 0.39 (−20 °C), 0.64 (0 °C), 0.68 (20 °C), 0.77 (50 °C) yielding ln K' = −3925 (1/T) + 18.8 (R^2 = 0.96).

Reaction of 2 with Olefins. The photoisomerization of the alkenes (*cis*-hex-2-ene to *trans*-hex-2-ene or 2,4-dimethylpenta-1,3-diene to 2,4-dimethylpenta-2,3-diene as examples) was prevented by wrapping the Schlenk tubes in aluminum foil. Tubes were capped and sealed with Parafilm to reduce evaporation of products. Celite, not silica gel, was used for product extraction in order to prevent σ-tropic rearrangements.[48]

With Hex-1-ene. Cp*IrB$_4$H$_9$ (10 mg, 2.6 10^{-5} mol) and Mo(tol)-(CO)$_3$ (10 mg, 3.7 10^{-5} mol) were first dissolved in 1 mL of THF-d_8 and stirred 10 min at 50 °C to generate **2**. Then 0.3 mL of hex-1-ene (2.4 10^{-3} mol) was added. A slow color change from (light orange) to dark yellow is observed at room temperature, and the ^{1}H NMR reveals conversion to *cis*-hex-2-ene in amounts exceeding initial catalyst quantities. ^{1}H NMR spectra of the crude were used to follow the reaction (Supporting Information, Table A). Turnover numbers (TON) were estimated from the integrated intensities of the alkenic protons lying between 4.5 and 5.5 ppm: *cis*-hex-2-ene; 5.34 ppm 2 H, m, and hex-1-ene; 4.87 ppm 2 H terminal, m. The catalyst was renewed each day by adding Cp*IrB$_4$H$_9$ and Mo(tol)(CO)$_3$ until complete conversion was obtained. The data are presented in Table A in the Supporting Information. For confirmation addition of 1 mL of hexane and extraction by Celite permitted analysis by both ^{1}H and ^{13}C NMR. They showed by comparison with standard spectra, hex-1-ene, and the σ-tropic product, *cis*-hex-2-ene, as well as THF and hexane. In the absence of an aluminum foil light shield, a mixture of *trans*-hex-2-ene and *cis*-hex-2-ene was observed. The thermal isomerization of hex-1-ene requires harsher conditions than those employed here.[44,45]

With 2,5-Dimethylpenta-2,4-diene. A rapid color change (from light orange to dark yellow brown) was observed at 50 °C after addition of 0.1 mL of allene (7.2 mmol) to Cp*IrB$_4$H$_9$ (30 mg, 0.078 mmol) and Mo(tol)(CO)$_3$ (30 mg, 0.11 mmol) in 1 mL of THF-d_8. After 3 h addition of hexane (1 mL) was followed by extraction on Celite. ^{1}H and ^{13}C NMR of this material revealed the presence of the isoprene derivative (2,4-dimethylpenta-1,3-diene) in addition to the solvents (THF and hexane) and the starting tetramethylallene. The ^{1}H NMR spectra show 20% conversion and a TON = 18. Because of the proximity of the proton shifts of the terminal-methyl resonances, the ratio between the cumulene and σ-tropic product was obtained from the ^{13}C NMR. This measurement gives 12% conversion and a TON = 11. The σ-tropic product is also observed at room temperature albeit in lower yield (7% conversion based ^{1}H NMR for a TON = 6.5 in 3 h).

Computational Details. Density functional theory calculations were carried out on model compounds (non-methylated Cp instead of Cp*) using the Amsterdam Density Functional (ADF) program[49] developed by Baerends and co-workers.[50,51] Electron correlation was treated within the local density approximation (LDA) in the Vosko−Wilk−Nusair parametrization.[52] The nonlocal corrections of Becke and Perdew were added to the exchange and correlation energies, respectively.[53,54] The atom electronic configurations were described by a triple-ζ Slater-type orbital (STO) basis set for H 1s, B 2s and 2p, C 2s and 2p, O 2s and 2p, augmented with a 2p single-ζ polarization function for H atoms, with a 3d single-ζ polarization function for O, and with a 3d and a 4f single for B and C. The atom electronic configurations of the Mo, Ru, and Ir atoms were described by a triple-ζ STO for the outer nd and (n + 1)s orbitals. A single-ζ STO was used for the outer Mo and Ru 5p orbitals and the outer Ir 6p orbitals. The Mo basis set was augmented with a 4f polarization function. For all atoms, a frozen core approximation for the inner shells was used. Geometry optimizations were carried out using the analytical gradient method implemented by Verluis and Ziegler.[55] Relativistic corrections were added using the zeroth-order regular approximation scalar Hamiltonian.[56−58] Representations of the total electronic densities were done using MOLEKEL4.1.[59]

Acknowledgment. This work was supported by the National Science Foundation (CHE 0304008) and by an International Grant (INT02-31792) in cooperation with the CNRS, France (14559-CNRS-NSF). We thank the French CINES (Montpellier) and IDRIS (Orsay) for computing facilities.

Supporting Information Available: Molecular structure of **8**, R = Ph (Figure A), time dependence of the ^{11}B spectra (Figure B), catalytic isomerization of hexane (Table A), and the optimized Cartesian coordinates of **6′**, **7′**, **8′**, and [1-Cp-5,6,7,8-(CH$_3$)$_4$-*closo*-1,5,6,7,8-IrC$_4$B$_3$H$_3$RuCp]$^+$. This material is available free of charge via the Internet at http://pubs.acs.org.

JA068999Z

(48) Kropp, P. J.; Breton, G. W.; Craig, S. L.; Crawford, S. D.; Durland, W. F., Jr.; Jones, J. E., Raleigh, J. S. III. *J. Org. Chem.* **1995**, *60*, 4146.

(49) SCM. *ADF*, 2005.01 ed.; Theoretical Chemistry, Vrije Universiteit: Amsterdam, The Netherlands, 2005.

(50) Fonseca Guerra, C.; Snijders, J. G.; te Velde, G.; Baerends, E. J. *Theor. Chem. Acc.* **1998**, *99*, 391−403.

(51) te Velde, G.; Bickelhaupt, F. M.; Fonseca Guerra, C.; van Gisbergen, S. J. A.; Baerends, E. J.; Snijders, J. G.; Ziegler, T. *J. Comput. Chem.* **2001**, *22*, 931−967.

(52) Vosko, S. D.; Wilk, L.; Nusair, M. *Can. J. Chem.* **1990**, *58*, 1200−1211.

(53) Perdew, J. P. *Phys. Rev. B* **1986**, *34*, 7406.

(54) Becke, A. D. *Phys. Rev. A* **1988**, *38*, 3098−3100.

(55) Verluis, L.; Ziegler, T. *J. Chem. Phys.* **1988**, *88*, 322−328.

(56) van Lenthe, E.; Baerends, E. J.; Snijders, J. G. *J. Chem. Phys.* **1993**, *99*, 4597−4610.

(57) van Lenthe, E.; Baerends, E. J.; Snijders, J. G. *J. Chem. Phys.* **1994**, *101*, 9783−9792.

(58) van Lenthe, E.; van Leeuwen, R.; Baerends, E. J.; Snijders, J. G. *Int. J. Quantum Chem.* **1996**, *57*, 281−293.

(59) Flükiger, P.; Lüthi, H. P.; Portmann, S.; Weber, J. *MOLEKEL4.1*; Swiss Center for Scientific Computing: Manno, Switzerland, 2002.